Chinese Chemical Letters 36 (2025) 110385

Contents lists available at ScienceDirect

Chinese Chemical Letters

journal homepage: www.elsevier.com/locate/cclet

Tuning the ion-dipole interactions between fluoro and carbonyl (EC) by electrolyte design for stable lithium metal batteries

Guihuang Fang[a,b,1], Ying Liu[b,1], Yangyang Feng[b], Ying Pan[b], Hongwei Yang[a,*], Yongchuan Liu[b,*], Maoxiang Wu[b,*]

[a] Faculty of Metallurgy and Energy Engineering, Kunming University of Science and Technology, Kunming 650093, China
[b] Key Laboratory of Optoelectronic Materials Chemistry and Physics, Fujian Institute of Research on the Structure of Matter, Chinese Academy of Sciences, Fuzhou 350002, China

ARTICLE INFO

Article history:
Received 9 July 2024
Revised 22 July 2024
Accepted 29 August 2024
Available online 3 September 2024

Keywords:
Lithium-ion batteries
$LiMn_{0.8}Fe_{0.2}PO_4$
High-voltage
Solvation structure
Ethylene carbonate
Bis(2,2,2-trifluoroethyl) carbonate

ABSTRACT

Ethylene carbonate (EC) is the conventional and promising solvent to achieve high energy lithium metal battery. However, the innate low energy level of lowest unoccupied molecular orbital (LUMO) in EC makes it incompatible with lithium metal, causing uncontrolled lithium growth and low Coulombic efficiency (CE). Herein, we introduced bis(2,2,2-trifluoroethyl) carbonate (TFEC), a carbonate with a strong electron-withdrawing effect (-CF_3), which enhances the stability of EC at electrode interface by reducing ion-dipole interactions between Li^+ and EC. As the interaction between Li and EC weakens, TFEC and more PF_6^- anions coordinate with Li^+, promoting the formation of contact ion pairs (CIPs) and aggregates (AGGs), thereby increasing the inorganic composition within the solid electrolyte interphase. Additionally, the distinct solvated sheath structure favors the decomposition of fluorinated solvents and PF_6^- anions, forming inorganic-rich electrode-electrolyte interfaces (SEI and CEI), thereby ensuring high stability for both the Li anode and high-voltage cathode. Hence, when applied in the full-cell Li||$LiMn_{0.8}Fe_{0.2}PO_4$, it displays consistent cycling performance, exhibiting minimal capacity decay with a retention rate of 62.5% after 800 cycles, substantially surpassing that of cells using base electrolytes (29.8%).

The development of cutting-edge technologies to fulfill the demanding energy density and safety standards of lithium-ion batteries (LIBs) is essential for the rapidly expanding electric vehicles and grid storage sectors [1,2]. Recently, Li-metal batteries (LMBs) have garnered interest due to the high specific capacity (3680 mAh/g) and low redox potential (-3.04 V *vs.* SHE) offered by the Li anode [3,4]. Regrettably, the formation of Li dendrites during the charging process has resulted in safety hazards like fires and explosions [5,6]. These concerns regarding safety have significantly restricted the progress of lithium metal batteries (LMBs).

However, the development of electrolytes has long lagged behind that of electrodes, and there is considerable attention on the research of electrolytes compatible with both positive and negative electrodes, among which carbonate and ether-based electrolytes are the most common [7-9]. In addition, ether solvents are considered to be more compatible with LMA among the frequently used solvents in LIBs electrolytes due to their high lowest unoccupied molecular orbital (LUMO) [10-12]. However, ethers have relatively low flash points, and gas generation takes place in ether-based electrolytes at a high voltage of approximately ≈4.6 V even in a LHCE [13,14], making them unsuitable for operation at very high voltages. Hence, carbonate electrolytes (*i.e.*, EC-based electrolyte), renowned for their robust oxidative stability and high flash points, have been extensively employed in commercial LIBs, making them the most cost-effective and appropriate choice for integration into high-voltage LMBs [15].

Ethylene carbonate (EC) occupies a prominent position in carbonate electrolytes, as the increase in its dielectric constant promotes the effective dissociation of lithium salts (such as $LiPF_6$), while its reduction can also facilitate the formation of the required SEI layer on the electrode surface, thereby enhancing stability [16,17]. However, the strong interaction between Li^+ and EC increases the desolvation energy barrier, leading to uncontrolled lithium growth due to poor quality of the interface layer and low CEs [18]. Meanwhile, EC preferentially contacts the electrode and undergoes decomposition, resulting in the formation of a weak SEI abundant in lithium carbonate (Li_2CO_3), lithium ethylene dicarbon-

* Corresponding authors.
E-mail addresses: hongweiy@kust.edu.cn (H. Yang), ycliu@fjirsm.ac.cn (Y. Liu), mxwu@fjirsm.ac.cn (M. Wu).
[1] These authors contributed equally to this work.

https://doi.org/10.1016/j.cclet.2024.110385
1001-8417/

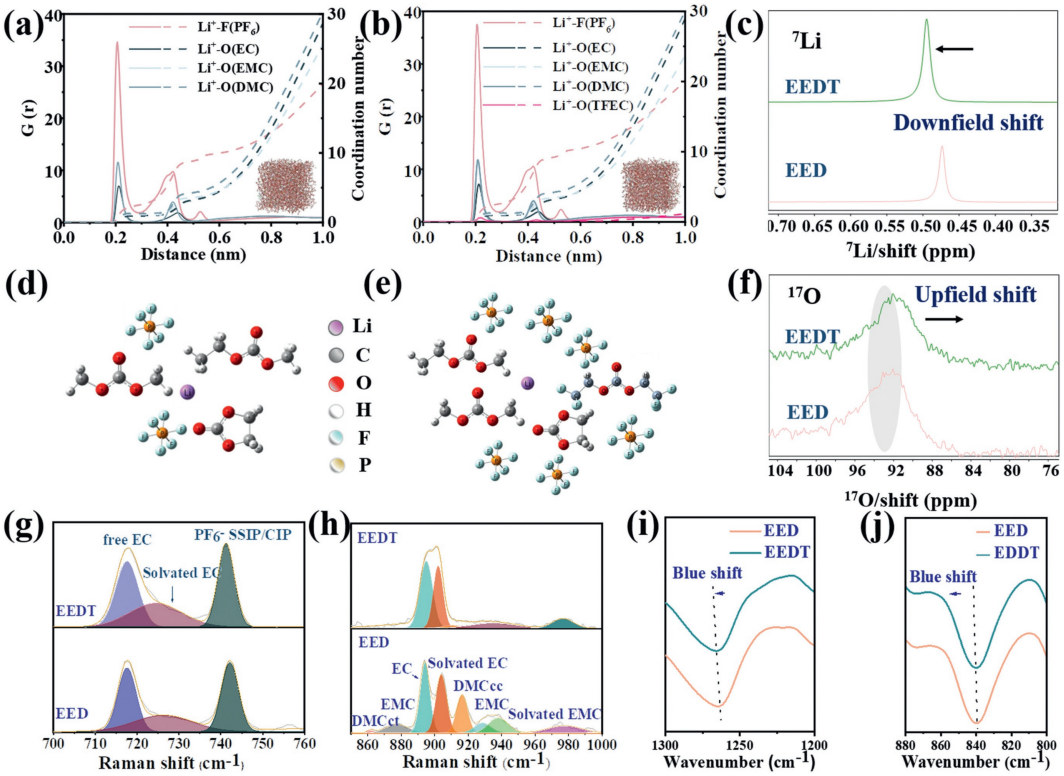

Fig. 1. The snapshot of MD simulation trajectories, radial distribution functions and coordination numbers in (a) EED and (b) EEDT electrolytes. (c) ^{7}Li NMR spectra. Schematics of the solvation structures of different electrolytes: (d) EED electrolyte, (e) EEDT electrolyte. (f) ^{17}O NMR spectra. (g, h) Raman spectra. (i, j) FTIR spectra.

ate (LEDC), and lithium ethylene monocarbonate (LEMC) [19-21]. Therefore, when designing EC-based electrolytes, it is essential to concurrently induce a protective solid-electrolyte interface by modulating the solvation structure. Given that the solvation structure of Li^+ is influenced by the competition between different solvents and anions for Li^+ coordination, it is feasible to reshape the solvation structure of Li^+ by modifying its coordination configuration.

In this study, we introduced bis(2,2,2-trifluoroethyl) carbonate (TFEC), a carbonate with weak solvation capability. The strong electron-withdrawing effect of the fluorine atom in TFEC (-CF_3 group) reduces the electron cloud density around the oxygen atom of the carbonyl (carbonate) group, weakening the interaction strength between Li and EC. This leads to more participation of PF_6^- anions and TFEC in the solvation structure of Li^+, promoting the formation of SEI rich in -CF_3 and LiF. At the same time, it enhances the stability and uniformity of CEI. Therefore, the Li||$LiMn_{0.8}Fe_{0.2}PO_4$ full cell exhibits a stable cycling performance showing limit capacity decay with a capacity retention of 62.5% after 800 cycles, which is far higher than those of the base electrolytes (29.8%). In addition, under the TFEC electrolyte system, Li||Li symmetric cells exhibit excellent long-term cycling stability, sustaining 800 h at a current density of 0.5 mA/cm^2 and a capacity of 0.5 mAh/cm^2.

The base electrolyte consists of 1.0 mol/L $LiPF_6$ dissolved in the mixed solvents of EC, ethyl methyl carbonate (EMC), and dimethyl carbonate (DMC) with a quality ration of 1:1:1, denoted as the EED electrolyte. The TFEC were added to the above base electrolytes, denoted as the EEDT electrolyte. The physical properties of EC, DMC, EMC, and TFEC are shown in Table S1 (Supporting information). The ionic conductivity of the EEDT electrolyte (10.90 mS/cm) shows a slight deviation from that of the EED electrolyte (11.48 mS/cm), as shown in Fig. S1 (Supporting information).

To further estimate the rationality of using the solvating power of solvents as a solvent indicator, we discuss the DFT calculations, which are used to study the electronic surface potentia (ESP) distribution and binding energy of solvents (Figs. S2a and b in Supporting information), where the absolute value of the binding energy for TFEC-Li^+ (-0.087 eV) is lower compared to EC-Li^+ (-0.207 eV), DMC-Li^+ (-0.225 eV), and EMC-Li^+ (-0.205 eV). This indicates that the strength of the ion-dipole interaction between TFEC and Li^+ is weaker than that of the other solvents studied. This implies that TFEC has a lower solvating power in terms of its ability to effectively solvate or interact with Li^+ ions. In addition, DFT calculations have revealed that TFEC has the lowest highest occupied molecular orbital (HOMO) compared to the other three solvents (Fig. S2c in Supporting information). This suggests that the free fluorinated carbonate solvent possesses a greater capability to resist oxidation.

Molecular dynamics (MD) simulations were performed to obtain a more profound understanding of the solvation sheath surrounding Li^+ ions (Figs. 1a and b). The radial distribution functions (RDFs) depicted in Figs. S3a and b (Supporting information), indicate that the intensity of Li-F(PF_6) in the EED electrolyte are weaker compared to those in the EEDT electrolyte, indicating the interaction between Li^+ and F(PF_6) ions becomes stronger with the addition of TFEC. This is beneficial as it helps reduce the decomposition of electrolyte, leading to the formation of the PF_6^- anion-derived interfacial layer that is enriched in fluorine [22]. Furthermore, the Li-O(TFEC) peak in the RDF profile is observed, suggesting that TFEC is participation in the Li^+ solvation structure. This result is consistent with the previous DFT calculations observations. Based on the results, the solvation structure of the EEDT electrolyte has been visually represented in Fig. 1d, with that of the conventional electrolyte (EED) shown in Fig. 1e for comparison.To further examine the influence of TFEC on the local environment of Li^+ in the electrolyte, ^{17}O nuclear magnetic resonance (NMR) spectroscopy was conducted. Fig. 1f demonstrates an upfield shift, which suggests an increase in electron density around oxygen (O)

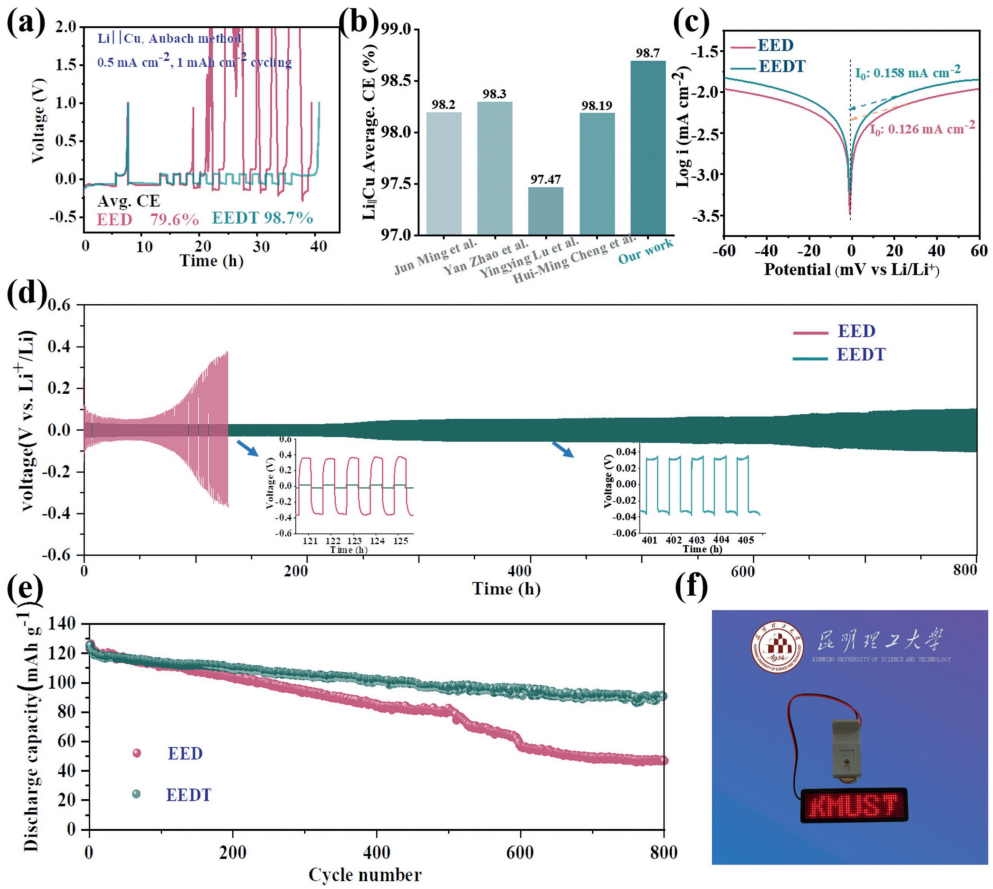

Fig. 2. Electrochemical behavior of different electrolytes. (a) CEs of Li stripping/plating in Li||Cu cells in different electrolytes at 0.5 mA/cm^2 with a capacity of 1 mAh/cm^2. (b) The comparison of CEs our Li||Cu cells and those of other research teams. (c) Tafel plots of Li||Li cells before galvanostatic cycling. (d) Long-term cycling of Li||Li symmetric cells. (e) Cycling performance of the Li||$LiMn_{0.8}Fe_{0.2}PO_4$ full cells. (f) The anti-polarization resistance test of the studied electrolytes involved two 800th cells in EEDT electrolyte configured in a KMUST pattern for LED lighting.

in solvent upon the addition of TFEC. This is further confirmed by the ^{7}Li NMR (Fig. 1c), where with EEDT electrolyte demonstrates a greater downfield shift (*i.e.*, more negative) compared to the EED electrolyte. This can be attributed to the weak solvation ability of TFEC, which reduces the interaction between Li^+ and the solvent, allowing more anions to squeeze into the primary solvation shell [23-25]. This observation validates the previous DFT and MD simulations results.

To gain a deeper understanding of the solvation structures in EED and EEDT electrolytes, we utilized Raman and ATR-FTIR analysis (Figs. 1g-j). Specifically, the stretching vibration at approximately ~720 and ~894 cm^{-1} could be attributed to free EC molecules, while the bands around ~730 and ~905 cm^{-1} are associated with solvated EC species [26,27]. Besides, DMC exhibits two primary conformations in the electrolyte: *cis-cis* (cc) and *cis-trans* (ct) [28], the bands at ~862 and ~917 cm^{-1} belonged to the pure DMC (ct) and DMC (cc) components, the bands at ~875 and ~934 cm^{-1} belonged to the solvated DMC (ct) and DMC (cc) components. In addition, the bands at ~938 and ~934 cm^{-1} belonged to the free EMC and solvated EMC, respectively [29,30]. It is important to note that the addition of TFEC leads to significant changes in the proportion of EC, DMC, and EMC molecules. Specifically, the presence of free EC, EMC, and DMC decreases or even disappears, giving way to the formation of solvated EC, EMC, and DMC species (Figs. 1g and h). Further analysis reveals the presence of two bands at approximately 740 and 745 cm^{-1}, suggesting an increased presence of CIPs within the EEDT electrolyte [30]. Moreover, this phenomenon can also be observed in the shift of peak positions in FTIR. Specifically, the bands ~1260 and 840 cm^{-1} associated with the coordination of Li^+ and solvents display a blue shift in the presence of TFEC (Figs. 1i and j, Fig. S3 in Supporting information) [31]. These spectral analyses indicate a weakening of the interaction between Li^+ and solvents in the solvation structure, while highlighting an enhancement in the interaction with the anion.

Further insights into the solvation behavior of electrolytes in different solutions can be gained by examining the performance of the lithium metal anode. When employing the Aurbach method [32], it is observed that the Li||Cu cell cycled at current density of 0.5 mA/cm^2 with constant areal capacity of 1 mAh/cm^2 utilizing the EEDT electrolyte exhibits superior reversibility (Fig. 2a). Moreover, our research illustrates that under similar conditions, our performance of the Li||Cu cell surpasses those of other research teams (Fig. 2b) [32-35]. Meanwhile, the Tafel curves show that the exchange current density of the EEDT electrolyte is relatively higher at 0.158 mA/cm^2 compared to 0.126 mA/cm^2 (Fig. 2c). A higher value for exchange current densities signifies greater interfacial charge-transfer kinetics and a reduced overpotential in the electrochemical reaction [35,36]. Moreover, the utilization of the EEDT electrolyte in the symmetric Li||Li cell results in remarkably low overpotentials and demonstrates excellent cycling stability throughout the lithium plating/stripping process when the areal capacity is maintained at 0.5 mAh/cm^2 under a current density of 0.5 mA/cm^2, lasting for over 800 h (Fig. 2d). These comprehensive results provide substantial evidence of the significant potential of EEDT electrolyte studied during long-term cycling tests, which are further corroborated by the subsequent evaluation of the Li||$LiMn_{0.8}Fe_{0.2}PO_4$ full cell cycling performance (Fig. 2e).

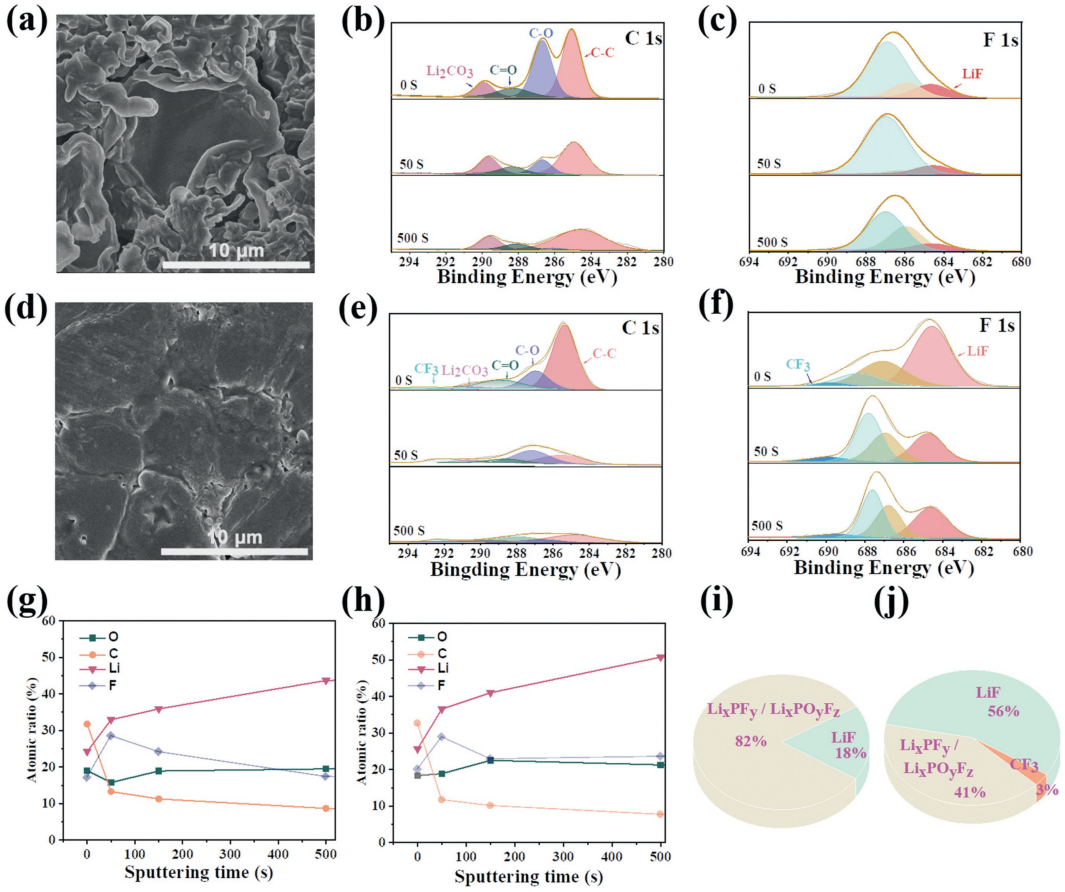

Fig. 3. The Top-view SEM images of the cycled Li anodes using different electrolytes in Li||$LiMn_{0.8}Fe_{0.2}PO_4$ cells after 800 cycles: (a) EED electrolyte, (b) EEDT electrolyte. SEI information obtained by in-depth XPS measurement on Li electrodes after 30 cycles in symmetric Li||Li cells. The XPS spectra of SEI formed on Li surface (c, e) using EED electrolyte and (d, f) using EEDT electrolyte are presented in columns, corresponding to certain depth after Ar^+ sputtering. Quantified atomic composition ratios of the SEI at different Ar^+ sputtering times and pie charts of fluorinated substances contained in SEI of the surface (sputtering time: 0 min) obtained from F 1s XPS spectra for (g, i) EED electrolyte and (h, j) using EEDT electrolyte.

The typical charge-discharge curves at different cycles for Li|| $LiMn_{0.8}Fe_{0.2}PO_4$ full cells in the EED and EEDT electrolyte are shown in Fig. S4 (Supporting information). Notably, at the 800^{th} cycle, the EED electrolyte exhibits significantly higher polarizations (Fig. S4a). This phenomenon is clearly depicted in Fig. 2e, which shows the cycle performance between 3.0 V and 4.5 V (*vs.* Li^+/Li). After 800 cycles, the full cell utilizing EEDT electrolyte demonstrates a significantly improved specific capacity of 90.6 mAh/g in comparison to the EED electrolyte (44.7 mAh/g), exhibiting much greater stability throughout the cycling process. Even after 800 cycles, when two cells are connected in parallel, the general power LED indicators loaded in them can still emit high brightness (Fig. 2f). Furthermore, electrochemical impedance spectra (EIS) are also included to examine the impact of EEDT electrolyte on the resistance of Li|| $LiMn_{0.8}Fe_{0.2}PO_4$ full cells (Fig. S5 in Supporting information). Fig. S5a reveals an interesting finding that the newly assembled full cells exhibit higher interfacial resistance in the EEDT electrolyte compared to the EED electrolyte. This observation corresponds well with the larger polarization observed in the first charge-discharge curves of the EEDT electrolyte (Fig. S4). Additionally, the impedance in the EED electrolyte surpasses 2500 Ohms, higher than the <1500 Ohms observed in the EEDT electrolyte after 800 cycles (Fig. S5c). The EIS results, combined with the aforementioned charge and discharge curves and cycling performance, demonstrate that the addition of TFEC effectively alleviates capacity degradation and enhances the movement of lithium ions and electrons.

To observe the effect of EEDT electrolyte on Li anodes during cycling process, the morphology of the cycled Li anodes recovered from practical Li||$LiMn_{0.8}Fe_{0.2}PO_4$ cells were characterized using scanning electron microscopy (SEM). The Li anode cycled in the EEDT electrolyte exhibited a dense and compact surface in Fig. S3d (Supporting information), with no visible surface cracks or evidence of Li dendrite growth observed. In stark contrast, when cycled in the EED electrolyte, the cycled Li anode exhibited a nonuniform and porous surface, prominently featuring the presence of Li dendrites (Fig. 3a). X-ray photoelectron spectroscopy (XPS) was utilized to analyze and identify the components of the SEI on cycled Li anodes, investigating the considerable contrast in surface morphology. The XPS analysis involved different etching times and was conducted on samples using EED and EEDT electrolytes (Figs. 3b and e). The outer layer of the SEI (sputtering time: 0 min) formed in both electrolytes comprised of both inorganic substances such as Li_2CO_3 and LiF, as well as organic compounds like $ROCO_2Li$ which are derived from the reduction of the electrolyte [37]. The presence of relatively high intensity of products, such as $ROCO_2Li$ and Li_2CO_3, was observed in the C 1s spectra (Fig. 3b) of EED electrolytes, indicating a significant occurrence of side reactions involving EC-based organic solvents [37]. Differences in electrolyte composition are clearly evident in the F 1s spectra obtained from the Li surface (Figs. 3c and f). The relative percentage of LiF is higher in EEDT electrolytes at 56%, compared to 18% in EED electrolytes (Figs. 3i and j). Furthermore, the atomic composition ratios at the lithium anode interface in the EEDT electrolyte indicate a higher

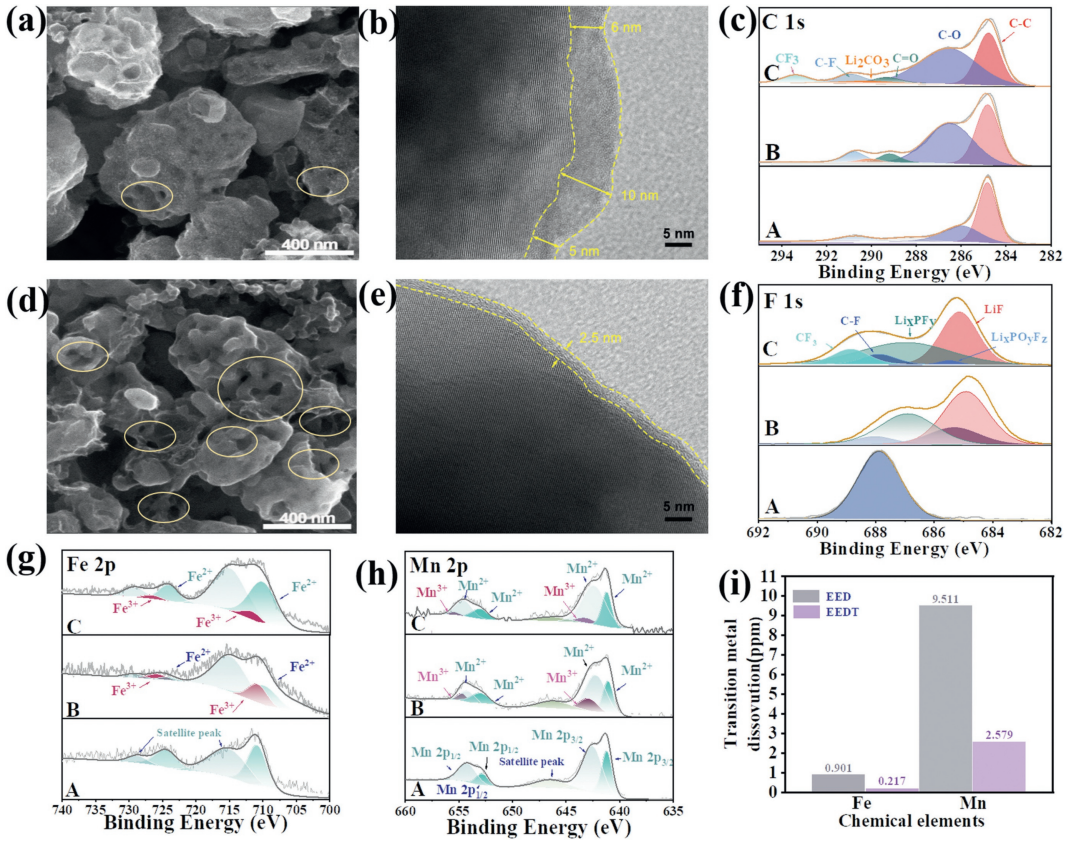

Fig. 4. SEM of the cycled $LiMn_{0.8}Fe_{0.2}PO_4$ cathode in various electrolytes after 800 cycles: (a) EED electrolyte, (d) EEDT electrolyte. HRTEM of the cycled $LiMn_{0.8}Fe_{0.2}PO_4$ cathodes in various electrolytes after 800 cycles: (b) EED electrolyte, (e) EEDT electrolyte. (c, f-h) The XPS spectra of $LiMn_{0.8}Fe_{0.2}PO_4$ cathodes in various electrolytes after 800 cycles: (A) uncycled, (B) after 800 cycles in EED electrolyte and (C) the TFEC-containing electrolyte (EEDT). (i) The dissolution content of Mn and Fe for the charged $LiMn_{0.8}Fe_{0.2}PO_4$ cathodes aged in the EED and EEDT electrolyte at room temperature.

fluorine content compared to the EED electrolyte (Figs. 3g and h), pointing towards the formation of a substantial inorganic SEI on the lithium anode surface. Notably, in the EEDT electrolyte (Figs. 3d and f), the additional peak at 293.0 eV (C 1s spectrum) and 688.6 eV (F 1s spectrum) corresponding to $-CF_3$ bonding are observed at various depths of the SEI [37,38]. The DFT calculations provide further evidence supporting this observation, showing that TFEC, possessing the lowest LUMO energy level compared to EC, EMC, and DMC (Fig. S2c in Supporting informaiton), selectively decomposes on the Li metal anode surface. Figs. 3g and h illustrate the atomic ratios of four selected elements on the cycled Li anodes, acquired at various depths. During the cycling of Li anodes in EED electrolytes, the inorganic component (represented by Li) within the SEI layer exhibits an initial increase and subsequently a decrease as the sputtering time is extended. Moreover, the uneven distribution of the four elements at the two depths within the SEI creates an inhomogeneous Li^+ flux and leads to non-uniform lithium deposition. This lack of uniformity ultimately negatively affects the cycling stability of the Li anodes over time (Fig. 3g). On the other hand, in stark contrast to the previous case, the SEI formed in the EEDT electrolyte demonstrates a nearly constant atomic ratio of the four elements at two distinct depths (Fig. 3h). The uniform internal composition of the SEI derived in the EEDT electrolyte imparts unique properties to the SEI layer. In addition, the presence of LiF on the SEI surface enhances the efficient distribution of lithium ions parallel to the interface and promotes uniform deposition of lithium during cycling processes. As a result, side reactions are minimized, leading to improved cycling performance.

A comparison between the two cathode SEM images reveals that the cycled $LiMn_{0.8}Fe_{0.2}PO_4$ cathode in the EED electrolyte exhibits severe blockage of pores, whereas in the electrolyte EEDT, the degree of blockage is noticeably reduced (Figs. 4a and d). The findings are consistent with the CEI thicknesses observed through high-resolution transmission electron microscopy (HRTEM) in Figs. 4b and e. Notably, the EEDT electrolyte yields a thinner and more uniform CEI layer, suggesting that the presence of TFEC effectively mitigates the continuous decomposition of electrolyte solvents. Moreover, the composition of the CEI layer formed on the $LiMn_{0.8}Fe_{0.2}PO_4$ further confirms the distinctions arising from the variances in electrolyte properties (Figs. 4c and f-h, Fig. S2c in Supporting information). A severe side reaction of organic solvents is indicated by the relatively high intensity of products, such as $ROCO_2Li$ and Li_2CO_3 [39], observed in the C 1s spectra of EED electrolytes. This indirectly indicates that TFEC can inhibit the decomposition of EC solvent [40,41]. Moreover, the $Li_xPO_yF_z$ peak (685.8 eV for F 1s, 534.2 eV for O 1s and 134.0 eV for P 2p in Fig. 4f and Fig. S6 in Supporting information) [42,43] is significantly weaker for the $LiMn_{0.8}Fe_{0.2}PO_4$ cathode cycled in the EEDT electrolyte compared to that in the EED electrolyte, indicating that less $Li_xPO_yF_z$ is generated in the EEDT electrolyte during cycling. In addition, we observed small peaks at 293.0 eV (C 1s) and 688.6 eV (F 1s), attributed to the $-CF_3$ group of TFEC, indicating the involvement of TFEC in building the CEI (Figs. 4c and f) [36]. Furthermore, the EEDT electrolyte effectively suppresses the dissolution of Mn and Fe from the $LiMn_{0.8}Fe_{0.2}PO_4$ cathode, as observed in the Fe 2p and Mn 2p spectra (Figs. 4g and h) [44]. The restrained degradation of $LiPF_6$, which results in the generation of scarce HF, is the primary factor responsible for the leaching of metals from $LiMn_{0.8}Fe_{0.2}PO_4$ cathode. Therefore, in order to provide evidence for the dissolution of the cathodes, we conducted a

simulation experiment. We aged the charged $LiMn_{0.8}Fe_{0.2}PO_4$ cathode at room temperature for 20 days in EED and EEDT electrolytes, and compared the dissolution content of Mn and Fe (Fig. 4i). It is evident that the EED electrolyte exhibits significantly higher levels of Mn and Fe dissolution compared to the containing TFEC electrolyte (EEDT), indicating that the presence of TFEC in the electrolyte effectively suppresses the dissolution of Mn and Fe from the $LiMn_{0.8}Fe_{0.2}PO_4$ cathode. The XPS spectra and inductive coupled plasma optical emission spectrometer (ICP) findings (Fig. 4i) are consistent with the observations obtainedfrom SEM, HRTEM, XRD and FTIR (Figs. S7 and S8 in Supporting information).These results indicate that TFEC can suppress the decomposition of solvent and lithium salt in the electrolyte during the charge-discharge cycle of $LiMn_{0.8}Fe_{0.2}PO_4$ cells, leading to a thin CEI formation on the surface of $LiMn_{0.8}Fe_{0.2}PO_4$ cathode and suppress the dissolution of transition metal, thereby enhancing the performance of lithium batteries.

This study demonstrates that TFEC enhances the stability of EC at electrode interface by leveraging the strong electron-withdrawing effect (-CF_3), which reduces the electron cloud density of the carbonyl oxygen and subsequently lowers the solvating power of solvents, leading to the creation of electrode-electrolyte interfaces rich in inorganic compounds (SEI and CEI), thereby enhancing the stability of both the lithium anode and high-voltage cathode. As expected, the Li||$LiMn_{0.8}Fe_{0.2}PO_4$ full cell demonstrates exceptional capacity retention at 62.5% after 800 cycles, significantly surpassing that of the base electrolytes (29.8%). Our work offers a new perspective on the application of EC-based electrolyte systems in high-voltage LMBs.

Declaration of competing interest

The authors declare that they have no known competing financial interests or personal relationships that could have appeared to influence the work reported in this paper.

CRediT authorship contribution statement

Guihuang Fang: Writing – review & editing, Writing – original draft, Supervision, Methodology, Investigation, Formal analysis, Data curation, Conceptualization. **Ying Liu:** Resources, Project administration, Methodology, Data curation. **Yangyang Feng:** Funding acquisition, Formal analysis, Data curation. **Ying Pan:** Formal analysis, Data curation. **Hongwei Yang:** Software, Resources, Project administration, Methodology. **Yongchuan Liu:** Project administration, Methodology. **Maoxiang Wu:** Resources, Investigation, Funding acquisition, Formal analysis.

Acknowledgments

This work is supported by National Natural Science Foundation of China (Nos. 12275274 and 22209182), the Fujian Provincial STS program supporting project of Chinese Academy of sciences (No. 2022T3001).

Supplementary materials

Supplementary material associated with this article can be found, in the online version, at doi:10.1016/j.cclet.2024.110385.

References

[1] J.M. Tarascon, M. Armand, Nature 414 (2001) 359–367.
[2] Y. Huang, J. Li, Adv. Energy Mater. 12 (2022) 48.
[3] X. Ren, P. Gao, L. Feng, W. Xu, Proc. Natl. Acad. Sci. U. S. A. 117 (2020) 28603–28613.
[4] J. Zhang, Y. Su, Y. Zhang, Nanoscale 12 (2020) 15528–15559.
[5] H. Kim, G. Jeong, Y. Kim, et al., Chem. Rev. 42 (2013) 9011–9034.
[6] W. Xu, J.Wang.F. Ding, et al., Energy Environ. Sci. 7 (2014) 513–537.
[7] G.H. Fang, Y. Pan, H.W. Yang, et al., J. Phys. Chem. C 128 (2024) 6877–6886.
[8] M. Du, J.Z. Guo, S.H. Zheng, et al., Chin. Chem. Lett. 34 (2023) 107706.
[9] H.Y. Wang, H.X. Chen, C. Chen, et al., Chin. Chem. Lett. 34 (2023) 107465.
[10] C. Wei, C. Liu, Y. Xiao, et al., Adv. Funct Mater. 33 (2023) 2314306.
[11] G.H Fang, W. Chen, H.S. Fang, et al., Chin. Chem. Lett. 35 (2024) 108799.
[12] Y. Liu, Y.Q. Chen, Y.S. Ling, et al., ACS Nano 17 (2023) 19625–19639.
[13] D. Zhang, Z. Liu, Y. Wu, et al., Adv. Sci. 9 (2022) 322.
[14] W. Xu, W. Dong, J. Zhou, et al., Adv. Sci. 6 (2024) 2400466.
[15] J. Zhang, W. Xu, J. Xiao, et al., Chem. Rev. 120 (2020) 13312.
[16] X. Zhang, X. Chen, X. Cheng, et al., Angew. Chem. Int. Ed. 57 (2018) 5301–5305.
[17] C. Yan, Y. Yao, X. Chen, et al., Angew. Chem. Int. Ed. 57 (2018) 14055–14059.
[18] X. Zheng, L. Huang, W. Luo, et al., ACS Energy Lett. 6 (2021) 2054.
[19] L. Hou, N. Yao, J. Xie, et al., Angew. Chem. Int. Ed. 61 (2022) 20.
[20] T.D. Pham, K.K. Lee, Small 17 (2021) 20.
[21] J. Wu, T. Zhou, B. Zhong, et al., ACS Appl. Mater. Interfaces 14 (2022) 27873–27881.
[22] J. Holoubek, M. Yu, S. Yu, et al., ACS Energy Lett. 5 (2020) 1438–1447.
[23] X. Yuan, T. Dong, J. Liu, et al., Angew. Chem. Int. Ed. 62 (2023) 1–12.
[24] C.V. Amanchukwu, Z. Yu, X. Kong, et al., J. Am. Chem. Soc. 142 (2020) 7393–7403.
[25] Z. Wang, Z. Sun, J. Li, et al., Chem. Soc. Rev. 50 (2021) 3178–3210.
[26] X. Liu, X. Shen, L. Luo, et al., ACS Energy Lett. 6 (2021) 4282–4290.
[27] O. Borodin, M. Olguin, P. Ganesh, et al., Phys. Chem. Chem. Phys. 18 (2016) 164–175.
[28] S. Uchida, T. Kiyobayashi, Phys. Chem. Chem. Phys. 23 (2021) 10875–10887.
[29] O. Borodin, G.D. Smith, J. Phys. Chem. B 113 (2009) 1763–1776.
[30] H. Su, Z. Chen, M. Li, et al., Adv. Mater. 35 (2023) 29.
[31] J. Ding, R. Xu, N. Yao, et al., Angew. Chem. Int. Ed. 60 (2021) 11442–11447.
[32] L. Zhao, Z. Wu, Z. Wang, et al., ACS Nano 16 (2022) 20891–20901.
[33] P. Xiao, Y. Zhao, Z. Piao, et al., Energy Environ. Sci. 15 (2022) 2435–2444.
[34] B.D. Adams, J. Zheng, X. Ren, et al., Adv. Energy Mater. 8 (2018) 1702097.
[35] W. Zhang, T. Yang, X. Liao, et al., Energy Storage Mater. 57 (2023) 2549 -259.
[36] S. Zhang, S. Li, X. Wang, et al., Nano Energy 114 (2023) 108639.
[37] W. Martin, Y. Tian, J. Xiao, J. Electrochem. Soc. 168 (2021) 060513.
[38] D.J. Yoo, S. Yang, K.J. Kim, et al., Angew. Chem. Int. Ed. 59 (2020) 14869–14876.
[39] S.H. Han, S.D. Han, O. Borodin, et al., J. Phys. Chem. C 119 (2015) 8492–8500.
[40] B. Horstmann, J. Shi, R. Amine, et al., Energy Environ. Sci. 14 (2021) 5289–5314.
[41] X. Zhang, X. Cheng, X. Chen, et al., Adv. Funct Mater. 27 (2017) 10.
[42] Z. Chang, Y. Qiao, H. Yang, et al., Angew. Chem. Int. Ed. 60 (2021) 15572–15581.
[43] K. Yoshida, M. Nakamura, Kazue Y, et al., J. Am. Chem. Soc. 133 (2011) 13121–13129.
[44] A Guéguen, L. Castro, R. Dedryvre, et al., J. Electrochem. Soc. 160 (2013) A387–A393.